

Thermal Sensors Fabricated by CMOS and Micromachining

Henry Baltes and Oliver Paul

Physical Electronics Laboratory, ETH Zürich,
8093 Zurich, Switzerland

(Received March 29, 1995; accepted December 29, 1995)

Key words: CMOS, micromachining, infrared sensor, power sensor, flow sensor, pressure sensor, thermal material properties

Integrated thermal sensors can be made by industrial CMOS IC technology combined with subsequent bulk or surface micromachining for thermal insulation. We review recent work on CMOS-based thermal radiation, AC power, mass flow, and pressure sensors with on-chip signal conditioning circuitry. We discuss diagnostic microstructures for the measurement of process-dependent thermal properties of CMOS materials.

1. Introduction

When the number of devices required is sufficiently large, it may be desirable to batch-manufacture sensors at low cost with high reliability and link them to integrated electronic circuitry. In this case the sensor designer will benefit from the knowledge of not only physical or chemical sensor effects and related materials, but also silicon IC fabrication technology and integrated circuitry. The task is to translate sensor effects into device structures that can be manufactured largely by standard industrial IC technology, which allows on-chip signal conditioning circuitry designed to enhance the sensor performance decisively.⁽¹⁾

Indeed, silicon sensor chips for temperature, optical radiation, and magnetic⁽²⁾ measurands can be fabricated by industrial CMOS or bipolar IC technology without further silicon processing. Microsensors for a number of thermal, mechanical or chemical⁽³⁾ measurands can be made by combining established IC technologies with additional, compatible processing steps specific to the sensor function. Preferably, such extra etching or deposition steps are performed by *post-processing*, i.e., processing after completion of the regular

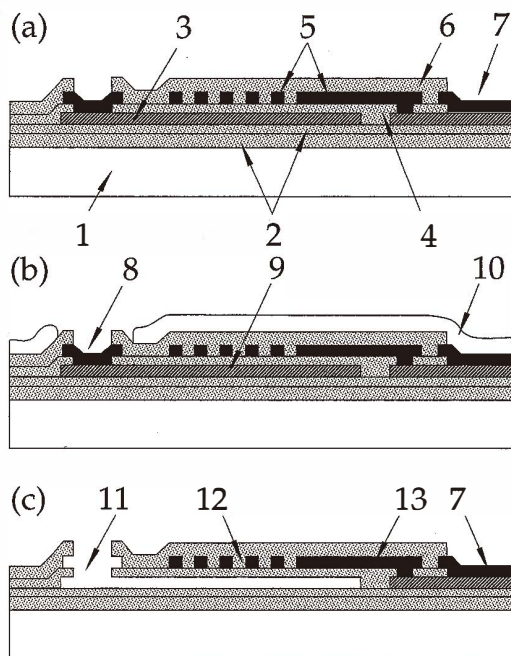


Fig. 1. Illustration of CMOS-compatible sacrificial metal etching. Cross section of pressure sensor after completion of CMOS IC process (a), photolithography (b), and metal etch (c). Silicon (1), silicon dioxide (2), first metal (3), intermetal dielectric (4), second metal (5), passivation (6), metal pad (7), entrance pad for metal etchant (8), sacrificial metal (9), photoresist (10), access port for gas (11), metal heater (12), heater interconnect (13).

dielectric membrane have been demonstrated.^(6,9) Figure 2 shows their schematic structure with an absorption area consisting of the silicon oxide/nitride passivation on an aluminum mirror above the CVD and thermal oxide layers. The overall membrane thickness is about $4 \mu\text{m}$. A temperature increase due to radiation focused on the absorption area is detected by an n-polysilicon/p-polysilicon thermopile ($300 \mu\text{V}/\text{K}$ Seebeck coefficient) with a total internal resistance of $2.5 \text{ M}\Omega$. Optimized devices reach $96 \text{ V}/\text{W}$ responsivity, $4.5 \times 10^7 \text{ cm} \sqrt{\text{Hz}}/\text{W}$ detectivity, and 31 ms rise time. The spectral response of the silicon oxide/nitride passivation approximately matches the radiation spectrum of an intruder with about $10 \mu\text{m}$ peak wavelength. The angular response of the sensor follows the cosine law. About 1 K temperature difference between the intruder and the background which results in a temperature increase of the sensor membrane of 0.01 K , can be resolved.

Figure 3 shows a micrograph of a chip with two sensor elements (each on a separate $720 \mu\text{m}$ by $720 \mu\text{m}$ membrane) and an operational amplifier. Since intrusion alarm detectors work in the frequency range of 0.1 to 10 Hz , $1/f$ noise cancellation is crucial. This can be achieved for example by the auto-zero technique. The low-noise amplifier consists

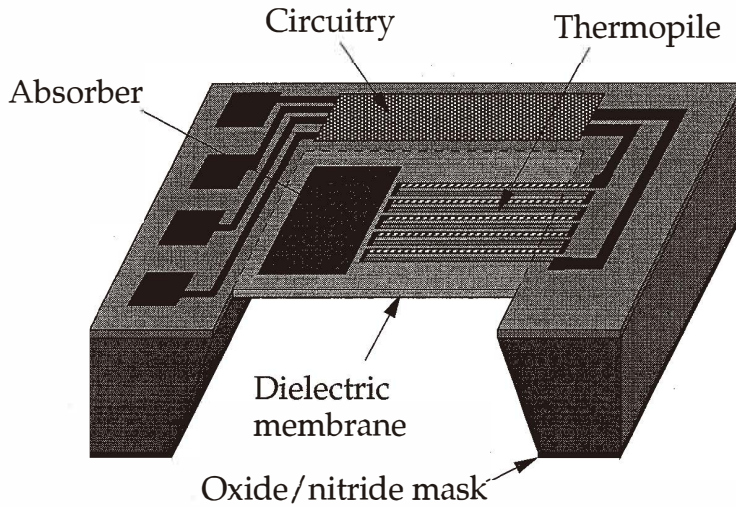


Fig. 2. Structure of CMOS-compatible thermoelectric infrared sensor on a closed membrane consisting of the CMOS dielectric layers with thermopile and metal mirror sandwiched in between.

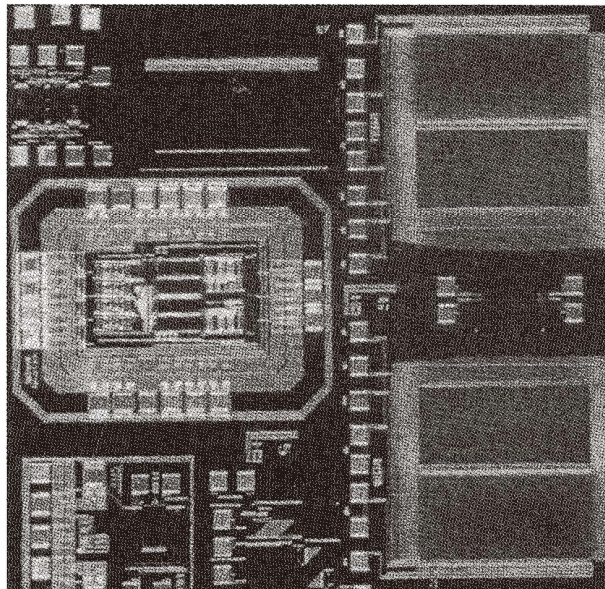


Fig. 3. Optical micrograph of dual infrared sensor with on-chip operational amplifier. The two sensor elements each consist of an absorbing area and an n-polysilicon/p-polysilicon thermopile on a $720\ \mu\text{m}$ by $720\ \mu\text{m}$ silicon oxide/nitride membrane.

of an operational transconductance amplifier followed by a multirate switched capacitor integrator.⁽¹³⁾ Both are based on the same folded cascade p-channel input stage. They differ in the biasing and the common mode feedback circuits. The transconductor has an additional differential pair for the offset and low-frequency noise compensation. The voltage gain is 60 dB. To overcome the high $1/f$ noise in MOSFET devices, one can also design a lateral bipolar device fabricated by a standard CMOS process. It is possible to reach equivalent input noise densities of less than $0.1 \mu\text{V}/\sqrt{\text{Hz}}$ for frequencies as low as 1 Hz.⁽⁶⁾

Prototypes were fabricated using a $1.2 \mu\text{m}$ CMOS IC process of AMS Austria Mikro Systeme on 100 mm wafers and a $2 \mu\text{m}$ CMOS IC process of EM Microelectronic Marin on 150 mm wafers. Subsequent to the latter process sequence, we performed the following steps on whole wafers: deposition of stress-compensated passivation nitride, deposition of etch protection layer on the wafer front, isotropic etch of the wafer back to achieve good adhesive conditions, deposition of the back nitride mask, photolithography on the wafer back, etch in a 6 M 95°C KOH solution, and dicing of the wafer. The overall membrane yield after dicing is higher than 98%. As a result of the stress-controlled deposition of the silicon nitride passivation,⁽⁹⁾ low-stress membranes with less than $0.1 \mu\text{m}$ buckling over the whole $720 \mu\text{m}$ by $720 \mu\text{m}$ area were achieved.

The same n-polysilicon/p-polysilicon thermopiles can be used for *CMOS thermal converters*⁽¹⁴⁾ which measure the mean square value of an unknown AC signal by thermoelectric conversion and contain signal conditioning circuitry on the same chip. Possible applications are microwave instrumentation and thermal voltage standards. Compensation of the nonlinearity at high power levels and of the dependence on the ambient temperature can be achieved by using two sensor elements in a first-order sigma-delta modulator.⁽¹⁴⁾

4. Thermal Gas Flow Sensor

Improved *open* and *closed* CMOS microstructures for the measurement of mass flow have been reported recently.⁽¹⁵⁾ As an example of an open structure, Fig. 4 shows a two-dimensional thermal gas flow sensor based on two crossed microbridges. The operation of the device is based on the flow-dependent heat transport from a central integrated heater into the surrounding gas. A temperature difference is generated by the flow between downstream and upstream locations on the device. Four integrated polysilicon resistors of $1.05 \text{ k}\Omega$ each, symmetrically located around the center of the suspended bridges, provide the heating power of a few mW required to operate the sensor. Temperature differences are measured with integrated polysilicon/aluminum thermopiles with cold contacts on the silicon substrate and hot contacts on the suspended structure. Two pairs of parallel thermopiles respond to the respective collinear velocity components of the gas flow. Each thermopile produces a thermovoltage of 1.21 mV/K .

Figure 5 shows the differential output signals of both thermopile pairs as a function of flow rate. The flow was forced through a 0.8-mm-high, 8-mm-wide, and 30-mm-long flow channel past the flow sensor mounted into the channel wall. One thermopile pair was oriented parallel, the other perpendicular to the direction of flow. For rates below 250 sccm

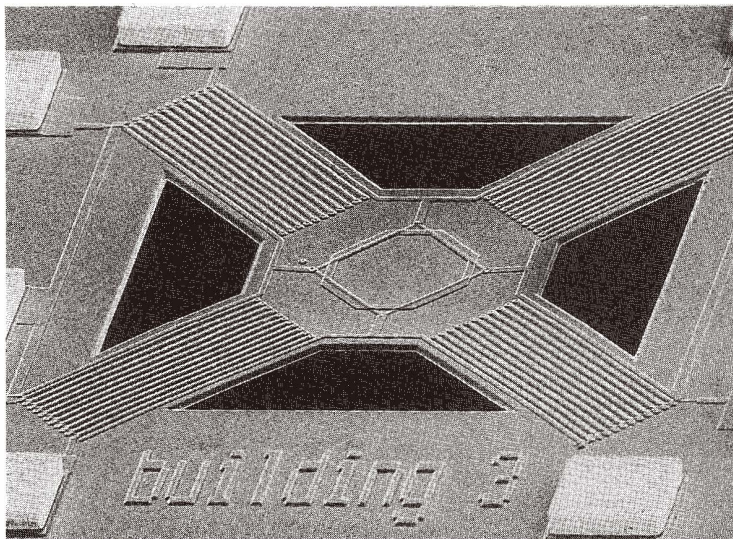


Fig. 4. SEM micrograph of thermal gas flow sensor for rate and direction measurements on a microbridge consisting of the CMOS dielectric layers with four heating resistors (in the center) and four thermopiles.

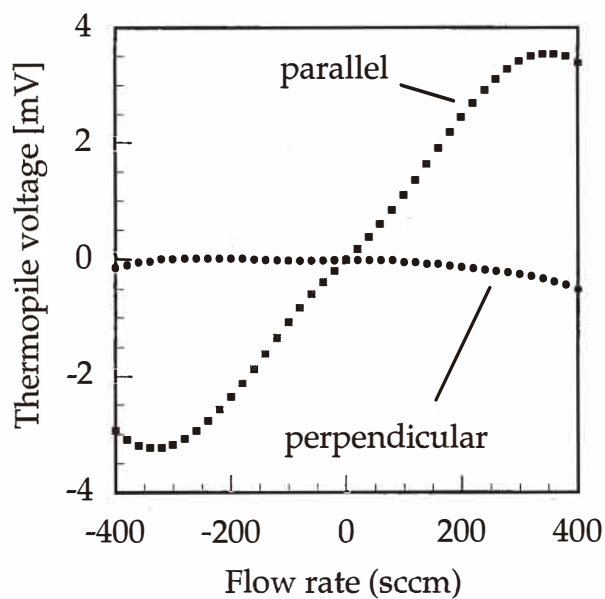


Fig. 5. Measured velocity response of the directional gas flow sensor shown in Fig. 4 in terms of the differential output voltages of the thermopile pairs oriented parallel and perpendicular to the gas flow direction.

the signal of the parallel thermopiles is linear with a sensitivity of $0.19 \text{ V W}^{-1} (\text{m/s})^{-1}$. This represents an appreciable improvement over previous micromachined flow sensors.^(5,16)

For vector measurements, the dependence of the corresponding output voltages U_x and U_y on the flow angle Φ at a flow rate of 50 sccm shows the expected harmonic behavior (Fig. 6). From U_x and U_y the thermally measured flow direction Φ_{meas} is calculated using $\Phi_{\text{meas}} = \arctan(U_y / U_x)$. An excellent correlation between Φ_{meas} and the geometrically determined Φ is found for this design; the mean deviation is only 1.7° .⁽¹⁵⁾

5. Vacuum Sensors

CMOS-based vacuum sensors have been demonstrated using bulk^(1,17) and surface⁽¹⁰⁻¹²⁾ micromachining. By bulk micromachining from the wafer front, beam-type thermoelectric and resonant microsensors can be combined on the same chip (see Fig. 7). In the first device, a polysilicon thermopile separated from a heating resistor by an air gap measures the temperature increase resulting from the heat conduction of the air. In the second, the air damping of a thermally excited vibrating beam is detected through piezoresistors integrated into its hinges.⁽¹⁸⁾ The two sensor principles are complementary and together cover

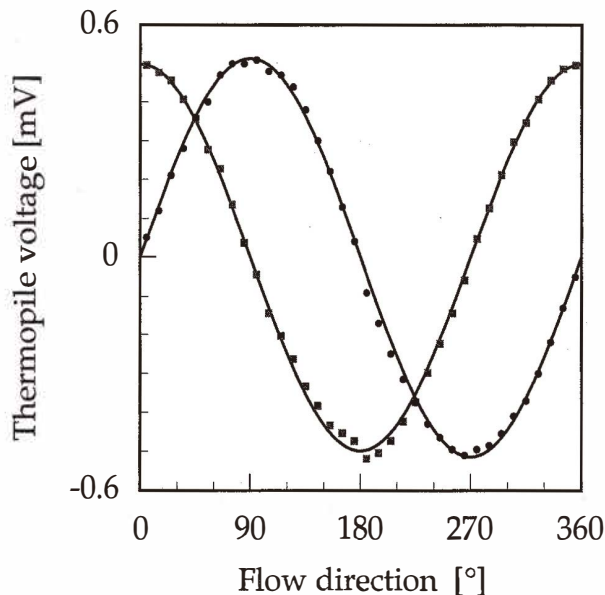


Fig. 6. Measured angular response (dots and squares) of the directional gas flow sensor shown in Fig. 4 in terms of the differential thermopile voltages as functions of gas flow direction, compared with harmonic fits (solid lines).

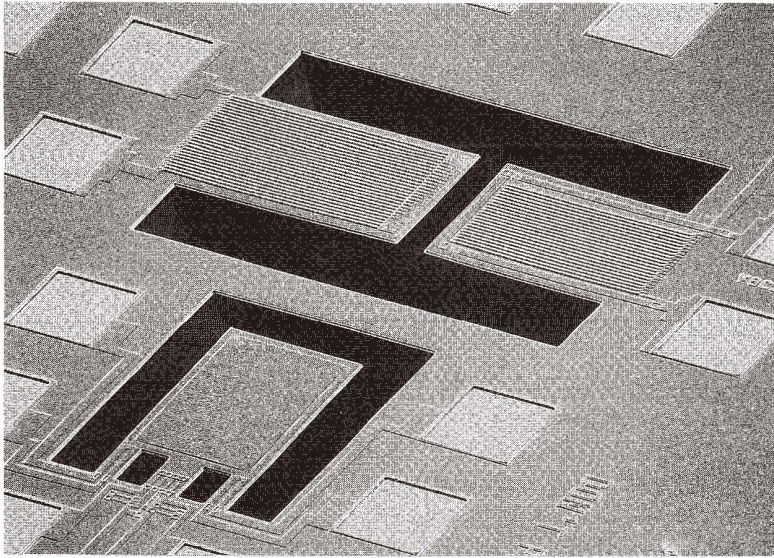


Fig. 7. SEM micrograph of thermally excited beam resonator (bottom) and thermoelectric pressure sensor (top) combined on the same CMOS chip. The thermoelectric sensor includes thermopiles on both beams and a heating resistor at the tip of the right beam.

the so-called Pirani range between 0.1 and 10^5 Pa.

A recent front-etched CMOS device spanning the pressure range from 10^2 to 10^6 Pa was fabricated based on two parallel polysilicon heater filaments.⁽¹⁹⁾ A different type of CMOS thermal pressure sensor for the same range⁽¹⁰⁻¹²⁾ has been fabricated by the sacrificial-metal surface-micromachining procedure outlined in section 2. The corresponding design cross section is given schematically in Fig. 1, while Fig. 8 shows a finished device with $200\ \mu\text{m}$ diameter. The sensor consists of a circular membrane composed of the intermetal isolation oxide and the passivation layer fabricated by the CMOS IC process. Sandwiched between the isolation oxide and the passivation is a $3\text{-}\mu\text{m}$ -wide meandering metal line, made of the second CMOS metal, which serves as a heater with a resistance of $50\ \Omega$. A $0.65\text{-}\mu\text{m}$ -wide air gap separates the membrane from the lower CMOS dielectrics and the substrate. During pressure measurements the air pressure in the gap is stabilized at the ambient value through eight lateral access ports. The operation of the sensor is based on the pressure-dependent heat conduction across the air gap. The power required to keep the membrane at a certain temperature above that of the substrate depends on the gas pressure. The measured thermal response agrees with the predictions of kinetic gas theory.⁽²⁰⁾

The above sensor was integrated with a pressure-insensitive reference structure and a simple read-out circuit consisting of an opamp and two n-channel transistors.⁽¹²⁾ Standard cells from the circuit library provided by the CMOS manufacturer were used. The circuit forces the sensor to track the resistance of the reference structure, which results in a

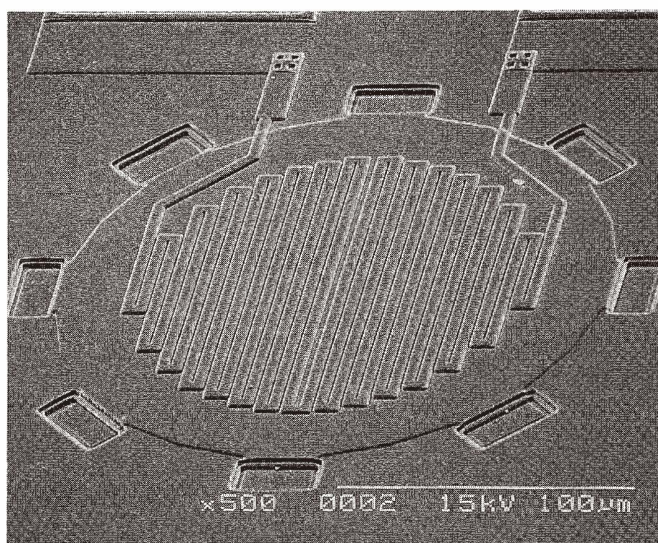


Fig. 8. SEM micrograph of surface-micromachined CMOS thermal pressure sensor with a circular membrane supporting an integrated meandering heater and eight access ports to the micromachined gap underneath the membrane.

constant temperature difference ΔT of the order of 6 K between sensor and reference. For the temperature stabilization of the pressure sensor the temperature coefficient of resistance (TC of R) of 0.34%/K of the heater was exploited. Figure 9 shows the corresponding output voltage as a function of air pressure. The microsystem shows maximum sensitivity between 10^2 and 10^6 Pa. In view of the unrestricted CMOS compatibility of the surface micromachining procedure used here, signal processing of the nonlinear output with dedicated CMOS circuitry can be incorporated easily.

6. Thermal Properties of CMOS Materials

The various responses of the microsensors discussed in the previous sections are determined by the thermal and electronic properties of their constitutive materials. In view of the “unconventional” uses of CMOS layers in microsensors, many sensor-relevant thin film properties are not routinely monitored in commercial IC processes. Knowledge of their values, however, is a prerequisite for thermal sensor design and, in particular, the optimization of such devices by numerical simulation. Table 1 summarizes the specific ways in which CMOS layers are used in the described thermal devices. Among the required material parameters are the thermal conductivities κ and heat capacities c of the individual layers. Of equal importance are electronic transport properties of the thermopile

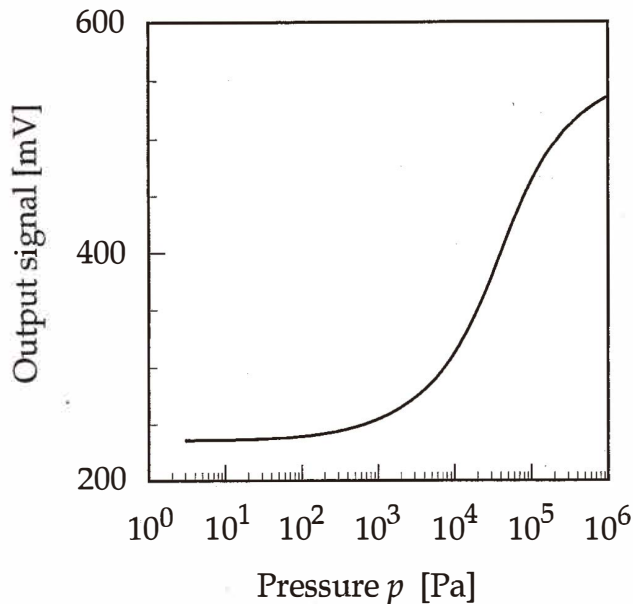


Fig. 9. Pressure response of a microsystem consisting of the thermal vacuum sensor shown in Fig. 8, a pressure-insensitive reference structure, and CMOS read-out circuitry.

materials, such as the Seebeck coefficient α , resistivity ρ , charge carrier densities n or p , and their respective temperature coefficients. In view of their process dependence, the properties have to be measured systematically for each IC process sequence used.

For this purpose we developed special CMOS-compatible micromachined diagnostic structures.⁽²¹⁻²⁴⁾ Each structure is optimized for one physical parameter while cross-sensitivities to other effects are minimized. Figure 10 shows a thermal microbeam used to measure the Seebeck coefficient of CMOS polysilicon against aluminum. The beam consists of the entire sandwich of CMOS dielectrics and contains an integrated heater, a temperature monitor, and a contacted sample of the characterized polysilicon layer. Other thermal structures have been designed to measure the thermal conductivities of all CMOS layers and heat capacities of some of them.^(21,22,24)

Table 2 lists measured thermal and electronic transport coefficients at 300 K. Results for the double-poly double-metal CMOS processes of Austria Mikro Systeme (AMS) and Microelectronic Marin (EM) with respective gate lengths of 1.2 and 2 μm are compiled. We routinely measure such properties in the temperature range from 100 to 420 K, which also allows derivation of the required temperature coefficients.

Table 1
Sensor-specific uses of CMOS IC layers for the thermal microsensors discussed in this paper.

Material	Use
Silicon dioxide	Thermal isolation Thermal mass Mechanical building block
Polysilicon	Thermopile component Heating resistor Temperature monitor Thermal conductor Thermal mass Mechanical building block
Metal layers	Thermopile component Thermal conductor Thermal mass Mechanical building block IR reflector
Passivation	Thermal isolation Thermal mass Mechanical building block IR absorber

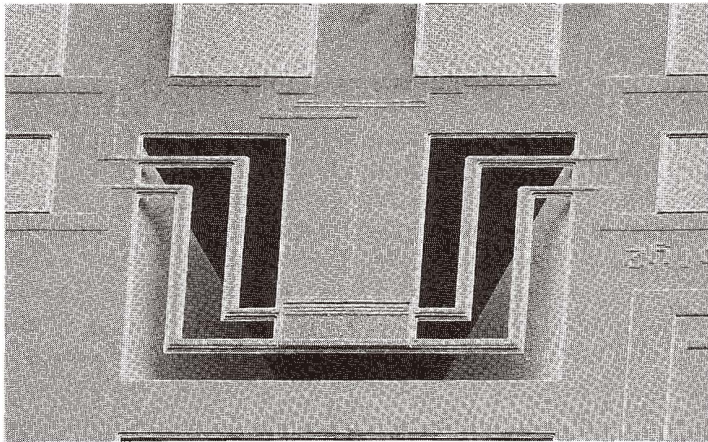


Fig. 10. SEM micrograph of a thermal diagnostic microstructure for measuring the Seebeck coefficient of CMOS polysilicon.

Table 2

Measured physical properties of materials in a 1.2 μm process of AMS Austria Mikro Systeme and a 2 μm process of EM Microelectronic Marin. Compiled properties are thermal conductivity κ , heat capacity c , Seebeck coefficient α , sheet resistance ρ , temperature coefficient of resistance (TC of R), and majority carrier densities n and p .

Material	Property		AMS	EM
SiO ₂ (thermal, CVD)	κ	[W/mK]	1.25 \pm 0.1	n.n.
	c (th.)	[J/cm ³ K]	1.05 \pm 0.1	n.n.
Poly-Si	κ_{n^+} , κ_{p^+}	[W/mK]	28 \pm 2, 19 \pm 2	17 \pm 2, 20 \pm 2
	α_{n^+} , α_{p^+}	[$\mu\text{V}/\text{K}$]	-120 \pm 5, 190 \pm 5	-111 \pm 5, 330 \pm 10
	ρ_{n^+} , ρ_{p^+}	[$\Omega/\text{Sq.}$]	25, 215	32, 425
	TC of R	[10 ⁻³ K ⁻¹]	0.860, -0.140	0.825, -0.586
	n^+ , p^+	[10 ²⁰ cm ⁻³]	3.4, 1.6	1.8, 0.33
Metal 1	κ	[W/mK]	194 \pm 8	250 \pm 10
	ρ	[m $\Omega/\text{Sq.}$]	65	44
	TC of R	[10 ⁻³ K ⁻¹]	2.96	4.38
Metal 2	κ_{n^+} , κ_{p^+}	[W/mK]	173 \pm 8	240 \pm 10
	ρ_{n^+} , ρ_{p^+}	[$\Omega/\text{Sq.}$]	36	29
	TC of R	[10 ⁻³ K ⁻¹]	3.01	4.28
Passivation	κ	[W/mK]	1.54 \pm 0.05	1.9 \pm 0.1
	c (th.)	[J/cm ³ K]	2.7 \pm 0.4	n.n.

7. Outlook

While the recent progress in thermal sensors made by CMOS IC technology combined with post-processing bulk or surface micromachining is impressive, it should be remembered that the translation of working prototypes into full-scale industrial production is not trivial. Even more difficult is the incorporation of the successful sensor chip into the final application system, in particular with respect to encapsulation.⁽²⁵⁾

While many CMOS manufacturers fabricate IC wafers and some are versed in CMOS-compatible micromachining, very few oversee the engineering of the whole system including reliability and electromagnetic compatibility, which is decisive for a successful final sensor product. On the research side this means that early collaboration between the sensor designer, CMOS manufacturer, and final system manufacturer is imperative.

Acknowledgments

The authors would like to thank Mr. D. Jaeggi, ETH Zurich, for contributing to section 3. The financial support of the Swiss Confederation through the Priority Program LESIT and the ESPRIT III Program of the European Union (BBW grant 93.0161) is gratefully acknowledged.

References

- 1 H. Baltes, O. Brand, J. G. Korvink, R. Lenggenhager and O. Paul: ESSDERC '94, ed. C. Hill, P. Ashburn (Editions Frontières, Gif-sur-Yvette, 1994) p. 273.
- 2 H. Baltes and R. Castagnetti: Magnetic Sensors, Semiconductor Sensors, ed. S. Sze (Wiley, New York, 1994) p. 205.
- 3 C. Cornila, R. Lenggenhager, P. Malcovati, H. Baltes, A. Hierlemann, G. Noetzel, U. Weimar and W. Göpel: Fifth Internat. Meeting on Chemical Sensors, Tech. Digest (University of Rome, Rome, 1994) p. 450.
- 4 H. Baltes: Sensors and Actuators **A 37-38** (1993) 51.
- 5 D. Moser: CMOS Flow Sensors, Ph. D. Thesis (ETH Zurich, Zurich, 1993).
- 6 R. Lenggenhager: CMOS Thermoelectric Infrared Sensors, Ph. D. Thesis (ETH Zurich, Zurich, 1994).
- 7 R. J. Reay, E. H. Klaassen and G. T. A. Kovacs: IEEE Electron Device Letts. **15** (1994) 399.
- 8 N. R. Swart, M. Parameswaran and A. Nathan: Transducers '93 Digest of Technical Papers (IEE Japan, Tokyo, 1993) 750.
- 9 R. Lenggenhager, D. Jaeggi, P. Malcovati, H. Duran, H. Baltes and E. Doering: IEDM '94 Technical Digest (IEEE, Piscataway, 1994) 531.
- 10 O. Paul and H. Baltes: Sensors and Materials **6** (1994) 245.
- 11 O. Paul and H. Baltes: Sensors and Actuators **A 46-47** (1995) 143.
- 12 O. Paul, A. Häberli, P. Malcovati and H. Baltes: IEDM '94 Technical Digest (IEEE, Piscataway, 1994) 131.
- 13 P. Malcovati, C. Azeredo Leme, R. Lenggenhager, F. Maloberti and H. Baltes: Proc. IMTC '94 (IEEE, Piscataway, 1994) 664.
- 14 D. Jaeggi, C. Azeredo Leme, P. O'Leary and H. Baltes: Transducers '93 Digest of Technical Papers (IEE Japan, Tokyo, 1993) 462.
- 15 J. Robadey, O. Paul and H. Baltes: J. Micromech. Microeng. **8** (1995) 243.
- 16 D. Moser, R. Lenggenhager, G. Wachutka and H. Baltes: Sensors and Actuators **B 6** (1992) 165.
- 17 O. Brand, R. Lenggenhager and H. Baltes: IEDM '93 Technical Digest (IEEE, Piscataway, 1993) 195.
- 18 O. Brand, H. Baltes and U. Baldenweg: IEEE Trans. Electron Devices **40** (1993) 1745.
- 19 N. R. Swart and A. Nathan: IEDM '94 Technical Digest (IEEE, Piscataway, 1994) 135.
- 20 O. Paul, O. Brand, R. Lenggenhager and H. Baltes: J. Vac. Sci. Tech. **A 13** (June 1995) 503.
- 21 O. Paul and H. Baltes: J. Micromech. Microeng. **3** (1993) 110.
- 22 O. Paul, J. G. Korvink and H. Baltes: Sensors and Actuators **A 41-42** (1995) 161.
- 23 O. Paul and H. Baltes: Transducers '93 Digest of Technical Papers, (IEE Japan, Tokyo, 1993) 606.
- 24 M. von Arx, O. Paul and H. Baltes: Sensors and Actuators **A46-47** (1995) 428.
- 25 D. Schaudel: Mikrotechnische Sensoren und Aktoren in der Betriebsmesstechnik für die Verfahrenstechnik, presented at VDE-Kongress '94, (VDE, Munich, 1994).